International Research Journal of Engineering and Technology (IRJET) e-ISSN: 2395-0056
Volume: 05 Issue: 07 | July 2018 www.irjet.net p-ISSN: 2395-0072

Effect of the bucket angle on the static torque of Savonius wind turbine rotors: Numerical Study

Sarkar A. M. Balak[1], Khedr A. Halimeh[2], Mohammad R. ALhafez[3], Hüseyin Çamur [4], Youssef Kassem[5]

[1,2,3,4]Department of Mechanical Engineering, Engineering Faculty, Near East University, Nicosia, via Mersin-10, Turkey
[5]Department of Civil Engineering, Civil and Environmental Engineering Faculty, Near East University, Nicosia, via Mersin-10, Turkey

---

Abstract - *Wind energy is the fastest growing of all renewable energy resources. Savonius wind turbine is the simplest type of vertical axis rotor that has a relatively low efficiency. Due to its simple design and low construction cost, this rotor is mainly used for water pumping as well as wind power on small scale. The main goal of this work is to investigate the effect of bucket arc angel of unconventional Savonius wind rotors positioned at different orientations. Autodesk Simulation CFD analyses were conducted for every case to find out the static torque by the turbines for each orientation. Ten different models with bucket arc angel were designed for the current study to find the effect of bucket arc angle on the performance of unconventional Savonius wind rotors. The turbine was also tested for varying wind velocities of rage 3-10m/s for a constant orientation of turbine. Additionally, the Autodesk Simulation CFD was used to characterize the flow characteristics around the rotor including velocity and pressure distributions. Moreover, the effect of end plate on the aerodynamic performance of the unconventional Savonius rotor was studied. Based on the result, the rotor with bucket angle of 150° has the highest static torque value compared to other models*

Key Words: Aerodynamic characteristics, Autodesk Simulation CFD analyses, Bucket angle, Savonius rotor, static torque

1.INTRODUCTION

Numerous studies of the vertical axis wind turbine were carried out based upon the Savonius wind turbine invented in 1920s. A Savonius rotor is a drag-type turbine [1, 2]. The conventional Savonius wind rotor has an axis with two semi-circular buckets perpendicular to the wind direction. With the advantages of simple design and low construction cost, it is mainly used for different applications [3]. Otherwise, the design and analysis of this rotor have aroused a large credit, not only in research and academic communities but also in industrial appliances. In comparison to that of other kinds, the efficiency of Savonius rotor is lower. The reason of low efficiency mainly rests on the fact that one bucket moves against the wind when another one moves in the direction of the wind [4, 5].

Savonius rotor is related to torque and most investigations have been experimental and numerical studies about the aerodynamic characteristics, effects of blade geometries, and the optimization of Savonius wind turbine rotors based on an experimental study and numerical analysis [6-16]. For example, Akwa et al. [17] examined numerically the influence of the buckets overlap ratio of a Savonius wind rotor on the averaged moment and power coefficients, over complete cycles of operation. The results showed that the buckets overlap of the rotor indicates that the maximum device performance occurs for buckets overlap ratios with values close to 0.15. Driss et al. [18] investigated experimentally the external overlap ratios effect on the performance of a vertical axis wind rotor of the Savonius type. They concluded that with the increase of the external overlap value, the torque and power coefficients decrease. Mohamed et al. [19] studied several shapes of obstacles and deflectors placed in front of two and three blades Savonius turbine. A rounded deflector structure was placed in front of two counter-rotating turbines. Wenehenubun et al. [20] studied experimentally the effect of number of blades on the performance of the model of the Savonius type wind turbine. In addition, they investigated numerically the pressure distribution of the turbine. They reported that Savonius model with three blades has the best performance at high tip speed ratio.

Furthermore, numerical techniques have overwhelmingly used in the study of the curved blade Savonius wind rotors [21-25]. Regarding the numerical study using SolidWork flow simulations with the steady Reynolds average Navier-Stokes (k-ε RNG) model, some recent papers, simulated unconventional Savonius wind rotors. For example, Driss et al. [26] studied the bucket design effect on the turbulent flow around unconventional Savonius wind rotors. The study compared the different design of rotors characterized by the bucket arc angles equal to ψ=60°, ψ=75°, ψ=90° and ψ=130° when keeping constants the others geometrical parameters. It is observed that the depression zones increase with the increase of the bucket

arc angle ψ. Driss et al. [27] investigated numerically and experimentally the turbulent flow around a small incurved Savonius wind rotor. They obtained that the incurved Savonius wind rotor has an effect on the local characteristics. Frikha et al. [28] studied numerically and experimentally the effect of five configurations with the different number of stages on the performance of a Savonius rotor. Basing on the obtained results, the number of stages affects the aerodynamic behavior of the turbulent flow around the Savonius rotor. Moreover, it showed that the dynamic torque coefficient and the power coefficient increase when the number of stage increases.

On the basis of the previous studies, this study aims to investigate numerically the static torque of different bucket design at various wind speed with keeping constants the others geometrical parameters. Consequently, the main goal of this paper is to examine the effect of bucket angle on the performance of Savonius rotor. Various buckets of Savonius rotors are designed and examined numerically in Fluid Mechanics Laboratory at Mechanical Engineering Department, Faculty of Engineering, Near East University.

2. MATERIAL AND METHOD

Autodesk Simulation CFD analyses with SST k-ω turbulence model is used in this work, that implements Reynolds averaged Navier-Stokes equations.

2.1 Case Study

Figure1 proposes different designs of the Savonius wind rotor. This rotor is constituted by two half buckets characterized by the height H = 700 mm, the diameter d = 160mmand the thickness t = 3 mm. The two buckets are collected on a common axis, with a shaft diameter equal to s = 20 mm, and they are fixed within screws to make an angle equal to 180°. Keeping constants these parameters, the bucket arc angle can changes. In this paper, the considered bucket arc angles are equal to 80, 90, 100, 125 and 150° (Figure 1). The second case considers a conventional Savonius wind rotor.

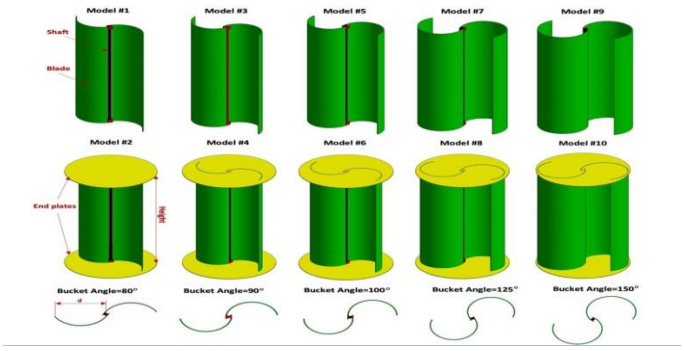

Fig -1: Savonius wind rotors

2.2 Mathematical Formulation

Autodesk Simulation CFD can handle both steady-state and transient analyses, and has several different options for modeling turbulence. Conservation of both mass and momentum is solved in all fluid flow cases, and in compressible flow or heat transfer cases. Consider a control volume which encloses a specified mass of fluid in a steady state flow field. Also consider a control surface around this volume, through which a certain mass of fluid enters and exits over a specific interval of time. If the flow is steady-state, these quantities are equal; therefore, there is no change in mass of the volume. This is the principle of continuity.

The continuity equation for unsteady, compressible flow is

$$\frac{\partial(\rho v_x)}{\partial x}+\frac{\partial(\rho v_y)}{\partial y}+\frac{\partial(\rho v_z)}{\partial z}+\frac{\partial \rho}{\partial t}=0 \qquad (1)$$

where v_x, v_y ,and v_z are the fluid velocities in the x, y, and z directions, respectively. And ρ is the density of the fluid. This equation states that the time rate at which mass increases within the control volume is equal to the net influx of mass across the control surface. Conservation of momentum can be written as

$$\frac{\partial}{\partial t}(\rho\vec{v})+\nabla\cdot(\rho\vec{v}\vec{v})=-\nabla p+\nabla\cdot(\vec{\tau})+\rho\vec{g}+\vec{F} \qquad (2)$$

Where $\rho\vec{g}$ and $\vec{F}$ are the gravitational and body forces, the stress tensor, $\bar{\tau}$ is.

$$\bar{\tau}=\mu\left[(\nabla\vec{v}+\nabla\vec{v}^{T})-\frac{2}{3}\nabla\cdot\vec{v}I\right] \qquad (3)$$

Fluid behavior can be characterized in terms of the fluid properties velocity vector u (with components u, v and w in the x, y, and z directions). Pressure p, density ρ, viscosity μ, heat conductivity k, and temperature T. Changes in these fluid properties can occur over space and time. Using CFD, these changes are calculated for small elements of the fluid, following the conservation laws of physics listed above. The changes are due to fluid flowing across the boundaries of the fluid element and can also be due to sources within the element producing changes in fluid properties.

Since it would be computationally prohibitive to model very small scale and high frequency fluctuations in fluid velocity seen in turbulent flow in production environments, time averaged methods of simulating turbulence effects have been derived. In these models, terms are introduced to simulate the average turbulent flow field, so that the small scale turbulent behavior does not have to be calculated explicitly by the Navier Stokes

equations. Instead, transport equations are solved in order to bring the model to closure and model the full range of turbulent flow scales. These are called Reynolds-average Navier Stokes (RANS) turbulence models which significantly reduce the processing power required and make turbulence modeling practical for a wide range of turbulent flow problems. In turbulence models that involve Reynolds averaging, the exact Navier- stokes flow solution is broken down into its varying and time averaged components. The general form of any scalar flow property can be given as

$$\phi = \bar{\phi} + \phi' \tag{4}$$

where $\bar{\phi}$ is the mean property value, and ϕ' is the varying value. If the time averaged values of the flow variables are substituted into the standard Navier Stokes equations, the Reynolds-averaged Navier-Stokes equations can be obtained:

$$\frac{\partial}{\partial t}(\rho u_i) + \frac{\partial}{\partial x_i}(\rho u_i \rho u_j) = -\frac{\partial p}{\partial x_i} + \frac{\partial}{\partial x_j}\left[\mu\left(\frac{\partial u_i}{\partial x_j} + \frac{\partial u_j}{\partial x_i} - \frac{2}{3}\delta_{ij}\frac{\partial u_l}{\partial x_l}\right)\right] + \frac{\partial}{\partial x_j}\left(-\rho\overline{u_i' u_j'}\right) \tag{5}$$

Two-equation RANS turbulence models use the Boussinesq hypothesis which states that the transfer of momentum generated by turbulent eddies can be modeled by an eddy viscosity, μ_t. The theory states that the Reynolds stress tensor, τ_{ij} is proportional to the rate of strain tensor $\bar{S}ij$, defined as

$$\bar{S}ij = \frac{1}{2}\left(\frac{\partial \bar{u}_i}{\partial x_j} + \frac{\partial \bar{u}_j}{\partial x_i}\right) \tag{6}$$

They can be modified as

$$\tau_{ij} = 2\mu_t 2\bar{S}ij - \frac{2}{3}k\delta_{ij} \tag{7}$$

This can also be written as

$$-\rho\overline{u_i' u_j'} = \mu_t\left(\frac{\partial u_i}{\partial x_j} + \frac{\partial u_j}{\partial x_i}\right) - \frac{2}{3}\left(\rho k + \mu_t\frac{\partial u_k}{\partial x_k}\right)\delta_{ij} \tag{8}$$

Boussinesq assumption provides a method of calculating the turbulent viscosity at a low computational cost. However, its main disadvantage that the Reynolds stress tensor is proportional to the strain rate tensor. This is not strictly true and is in fact invalid for a range of flows including those with strong accelerations or high curvature. Models have been developed which attempt to address this shortcoming, such as the Realizable k − ε and SST k − ω models.

2.2.1 Realizable k − ε turbulence model

A member of the k − ε family of turbulence models, k − ε Realizable, was used for rotating zones. Advantages of the k − ε Realizable turbulence model over the standard k − ε turbulence model include improved performance in flows with recirculation, strong pressure gradients, flow separation, and non-reliance on an assumed relationship between the Reynolds stress tensor and the strain rate tensor.

The transport equations for k and ε in the Realizable k − ε model are given as.

$$\frac{\partial}{\partial t}(pk) + \frac{\partial}{\partial x_j}(\rho k u_j) = \frac{\partial}{\partial x_j}\left[\left(\mu + \frac{\mu_t}{\sigma_k}\right)\frac{\partial k}{\partial x_j}\right] + G_k + G_b - \rho\varepsilon - Y_M + S_k \tag{9}$$

and

$$\frac{\partial}{\partial t}(\rho\varepsilon) + \frac{\partial}{\partial x_j}(\rho\varepsilon u_j) = \frac{\partial}{\partial x_j}\left[\left(\mu + \frac{\mu_t}{\sigma_\varepsilon}\right)\frac{\partial \varepsilon}{\partial x_j}\right] + \rho C_1 S_\varepsilon - \rho C_2 \frac{\varepsilon^2}{k + \sqrt{v\varepsilon}} + C_{1\varepsilon}\frac{\varepsilon}{k}C_3 G_b + S_\varepsilon \tag{10}$$

Where

$$C_1 = max\left[0.43, \frac{\eta}{\eta + 5}\right], \quad \eta = S\frac{k}{\varepsilon} and S = \sqrt{2S_{ij}S_{ij}} \tag{11}$$

Major difference in the form of the Realizable$k - \varepsilon$ model versus that of the standard $k - \varepsilon$ model is in the determination of C_μ is not a constant. It is instead calculated from

$$C_\mu = \frac{1}{A_0 + A_S\frac{kU^*}{\varepsilon}} \tag{12}$$

Where

$$U^* = \sqrt{S_{ij}} \tag{13}$$

$$\tilde{\Omega}_{ij} = \Omega_{ij} - 2\varepsilon_{ijk}\omega_k \tag{14}$$

$$\Omega_{ij} = \bar{\Omega}_{ij} - \varepsilon_{ijk}\omega_k \tag{15}$$

2.2.2 SST k − ω turbulence model

Shear-stress transport (SST)$k - \omega$ turbulence model is a type of hybrid model, combining two models in order to

calculate flow in the near-wall region. It was designed in response to the problem of the $k-\varepsilon$ model's unsatisfactory near-wall performance for boundary layers with adverse pressure gradients. It uses a standard k − ε model to obtain flow properties in the free-stream (turbulent) flow region far from the wall, while using a modified k − ε model near the wall using the turbulence frequency ω as a second variable instead of turbulent kinetic energy dissipation term . It is expected that the boundary layer flow has a strong influence on the results, and properly modeling this near-wall flow could be important for accuracy of the calculations. Therefore, *SST* $k-\omega$turbulence model has also been chosen for CFD simulation in this project. This *SST* $k-\omega$ model is similar to the $k-\varepsilon$turbulence model, but instead of ε as the second variable, it uses a turbulence frequency variable ω, which is expressed as $\omega = {}^{\varepsilon}/_{k}$. *SST* $k-\omega$ model calculates Reynolds stresses in the same way as in the $k-\varepsilon$ model. The transport equation for turbulent kinetic energy k for the k − ω model is:

$$\frac{\partial(\rho k)}{\partial t}+\frac{\partial}{\partial x_i}(\rho U_i k) = \frac{\partial}{\partial x_i}\left[\left(\mu+\frac{\mu_t}{\sigma_k}\right) grad(k)\right] + P_k - \beta^*\rho k\omega \quad (16)$$

where $P_k = \left(2\mu_t \frac{\partial U_i}{\partial x_i}\cdot\frac{\partial U_i}{\partial x_i} - \frac{2}{3}\rho k\frac{\partial U_i}{\partial x_i}\delta_{ij}\right)$

The terms in the above equation are defined as the following:

$\frac{\partial(\rho k)}{\partial t}$: Transient term represents the accumulation of k (rate of change of k)

$\frac{\partial}{\partial x_i}(\rho U_i k)$: Convective transport represents the transport of k by convection

$\frac{\partial}{\partial x_i}\left[\left(\mu+\frac{\mu_t}{\sigma_k}\right) grad(k)\right]$: Diffusive transport represents the turbulent diffusion transport of k

P_k: Production term represents the rate of production of k

$\beta^*\rho k\omega$: Dissipation represents the rate of dissipation of k

The transport equation for turbulent frequency ω for the k − ω model is: $\frac{\partial\rho\omega}{\partial t}+\frac{\partial}{\partial x_i}(\rho U_i\omega) = \frac{\partial}{\partial x_i}\left[\left(\mu+\frac{\mu_t}{\sigma_{\omega,1}}\right) grad(\omega)\right] + \gamma_2\left(2\rho\frac{\partial U_i}{\partial x_j}\cdot\frac{\partial U_i}{\partial x_j} - \frac{2}{3}\rho\omega\frac{\partial U_i}{\partial x_j}\delta_{ij}\right) - \beta_2\rho\omega^2 + 2\frac{\rho}{\sigma_{\omega.2}\omega}\frac{\partial k}{\partial x_k}\frac{\partial\omega}{\partial x_k}$ (17)

where $\sigma_{\omega,1}$, γ_2 , β_2 , and $\sigma_{\omega.2}$ are constants.

The general description for each of the terms in the above equation are the usual terms for accumulation, convection, diffusion, production, and dissipation of . Last term is called a 'cross-diffusion' term, an additional source term, and has a role in the transition of the modeling from ε to ω.

2.3 Boundary Conditions

The computational domain is defined by the interior volume of the rectangular shaped block with dimensions of 1200mm×1200mm×2400mm by two planes as shown in Figure 2. The boundary condition is required anywhere fluid enters or exits the system and can be set as a pressure, mass flow, volume flow or velocity. In the present application, the inlet boundary condition was wind speed, which was ranging between 3 to 10 m/s. For the outlet pressure, we take a value of p = 101325 Pa; which means that at this zone the fluid exits the model to an area of an atmospheric pressure. Knowing that the walls of the wind tunnel and the Savonius rotor shape are suspended from our computational domain, the walls of our computational domain are considered as wall boundary conditions.

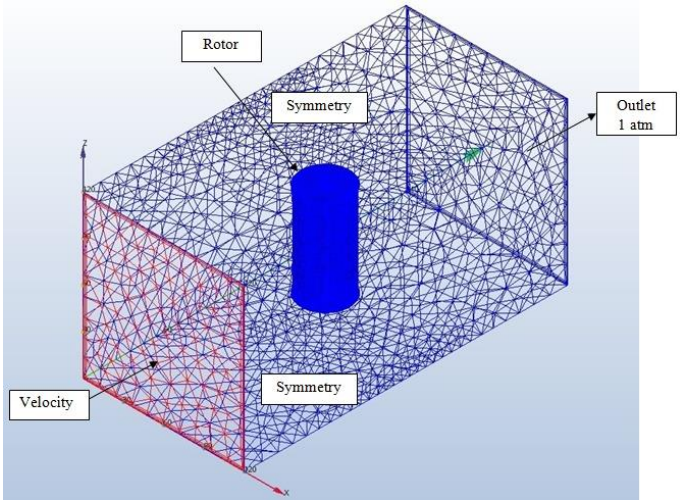

Fig -2: Computational domain and mesh for rotor models

2.3 Mesh

A grid sensitivity analysis was done to reduce the computational time and guarantee a minimum discretization error from experimental results. In this section, different grids on model with various element sizes were investigated and the optimal grid size was evaluated. Then the validity of the analysis was checked by comparison the numerically calculated static torque with experimental results [29].

Table 1 indicates the obtained error from comparing the calculated results with experimental ones in different

wind speeds. Results indicate a small dependence on grid resolution and by considering run time of modeling; cell numbers around 170216 have a good agreement with experimental results of ref [29].

Table -1: Calculated errors from comparison of numerical and experimental results [29]

Wind speed [m/s]	Cells number	Torque [N.m] (numerical)	Torque [N.m] [56]	Absolute Error [%]
6	18975	0.0166	0.0093	78.49
6.5	19560	0.0198	0.0142	39.43
7.27	20117	0.0242	0.0219	10.50
8.23	20943	0.0310	0.0363	14.60
9.21	170216	0.0383	0.0443	13.54
9.88	170216	0.0440	0.0474	7.17
10.17	170216	0.0475	0.0397	19.64

The grid independence test was made for improvement of the results by successively using smaller cell sizes grid. The stability of the results depends largely on the grid's resolution. The grid density is refined up to a certain limit, but beyond this limit, called the grid independent limit, the refinement ceases to significantly affect the results obtained. In fact, the different numbers of mesh cells are used, and the obtained results were compared with the experimental results, to find the optimal number of mesh cells required. It has been observed that when the resolution time increases, the number of mesh cells increases.

Figure 3 (an example) shows the various levels of refining using different mesh sizes for models. Each level was solved with the same set of input parameters. After a particular refining limit, the results cease to change. At this point, the grid independence in meshing is said to be achieved. Here, the successful achieved cells are 170216.

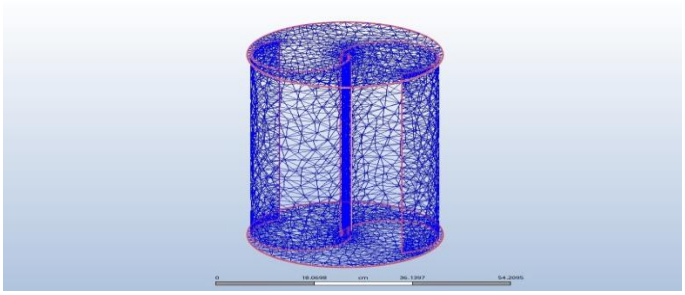

Fig -3: Mesh for rotor models used in this study

3. RESULTS AND DISCUSSION

3.1 Static torque of the rotors

Results of this study indicated the relationship between wind speeds and static torque as shown in Figure 4 and tabulated in Table 2. It is observed that the models with end plates have the higher static torque value than other models. Additionally, it can be seen that as the bucket angle increases, the static torque of the model increases also i.e., Model with bucket angle of 150° has the highest static torque values at different wind speed.

Figure 4(a) shows that Model 9 has maximum power compared to other models (Model 1, 3, 5, and 7). In addition, it is noticed that Model 5 with bucket angle of 100° and model 3 with bucket angle of 90°, which can considered as classical Savonius wind turbine have almost same static value at various speed as shown in Figure 4 and Table 2. For instant, at constant wind speed of 6m/s, the different between the static torque of Model 5 and Model 3 is about 0.0007 N.m, which can be considered as both models have same static value. Therefore, it can concluded that the effect of bucket angle with the range of 90° and 100° on the static torque value of the rotors can be neglected as shown in Figure 4(a), (b) and Table 2.

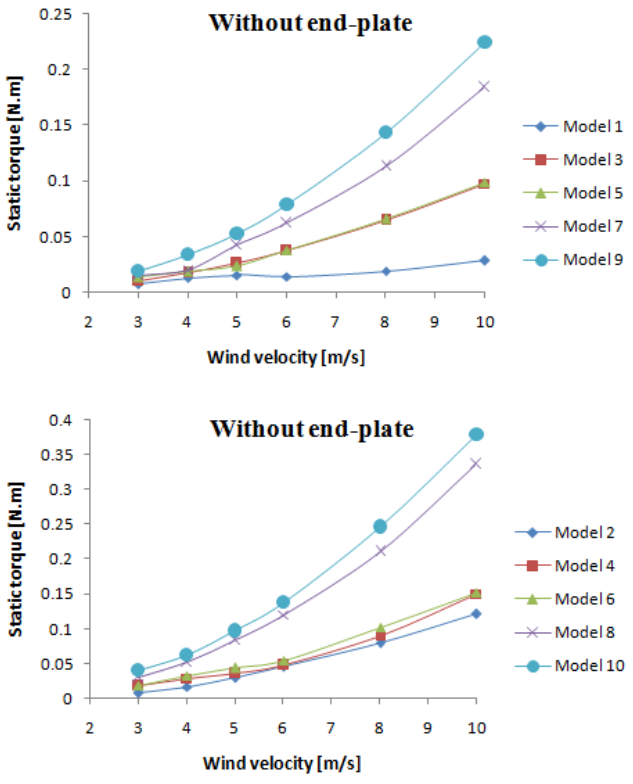

Fig -4: Static torque vs. wind speed

Table -2: Static torque values in N.m at various wind speeds

Velocity [m/s]	Without endplates				
	Model 1	**Model 3**	**Model 5**	**Model 7**	**Model 9**
3	0.0075	0.00994	0.0135	0.0146	0.0187
4	0.0128	0.0176	0.019	0.0205	0.0337
5	0.0156	0.02612	0.0237	0.0423	0.0528
6	0.0142	0.0373	0.038	0.062	0.0787
8	0.0192	0.0643	0.0655	0.1128	0.1436
10	0.0288	0.0978	0.0989	0.184	0.2243
Velocity [m/s]	**With endplates**				
	Model 2	**Model 4**	**Model 6**	**Model 8**	**Model 10**
3	0.0072	0.0183	0.0185	0.0292	0.0402
4	0.0167	0.0288	0.0326	0.0521	0.0626
5	0.0296	0.0353	0.0439	0.0829	0.0971
6	0.0463	0.0471	0.0548	0.1202	0.1377
8	0.0797	0.0902	0.1027	0.2105	0.2466
10	0.1214	0.1502	0.1525	0.3363	0.3792

3.2 aerodynamic characteristics of rotor

The aerodynamic characteristics of fluid flow i.e. velocity distribution and pressure distribution, of the models are studied. For example, the aerodynamic characteristics of model 9 with bucket angle of 150° are shown in Figures 5 and 6.

Figures 6, 8 and 10 show the distribution of the velocity distribution of the model 9 at different inlet velocities. While examining these results, it can be easily noted that the velocity is uniform in the inlet region. In fact, it is governed by the inlet velocity magnitude of the wind speed of 3, 4, 5, 6, 8, and 10 m/s. Then, the velocity decrease as we reach the near wall region of the turbine blades until it reaches the wall it becomes zero due to the *no-slip* condition. The velocity vectors slip over the surface to leave the blades from their edge at maximum velocity (turbulent flow) specified by the spectrum shown to the left of the figures. After that, a separation region is formed which is characterized by low velocity magnitude. As we get far from the walls of turbine blades the flow is regaining its uniform velocity where the separation gap is ended. A wake region is observed to appear in the rear region of the turbine blades this wake region is seen to be increasing as the inlet velocity increases the effect of wake region is that it decreases the drag of the turbine where it affects the torque negatively. The important parameter, which causes the turbine to rotate, is the separation gap between the two blades, which is a critical value in design of Savonius wind turbine.

Figures 5, 7 and 9 show the distribution of the pressure on the planes defined in the corresponded figures. According to these results, it has been noted that the static pressure is on its maximum in the intake and is globally uniform in the region away from the rotor. A brutal drop of the has been noted in the surfaces of the rear area of the blades of the rotor. This changes in pressure causes the adverse pressure to be formed in the rear area. As we move away from the rotor the pressure continues to increase to gain its value of atmospheric pressure since the outlet region is governed by the boundary condition of atmospheric pressure. The comparison between these results confirms that the bucket design have a direct effect on the static pressure distribution. In fact, as the bucket arc angle increases the pressure distributed drops in the concave intake bucket and concentrated in the convex of the intake bucket, which results in lower values of the negative pressure.

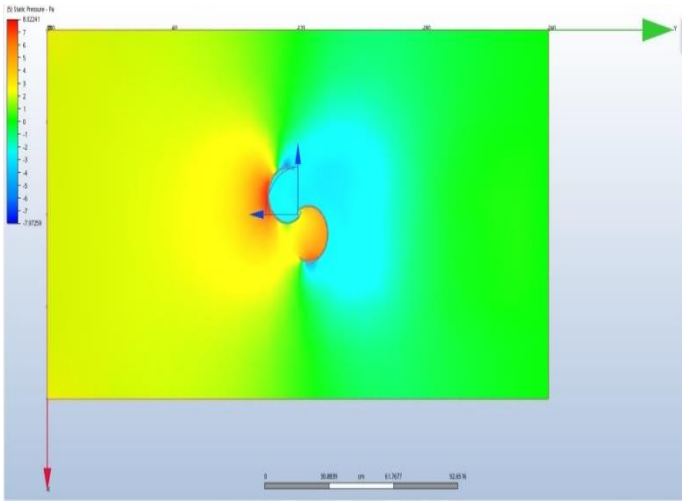

Fig -5: Pressure distribution of Model 9 at wind speed of 3m/s

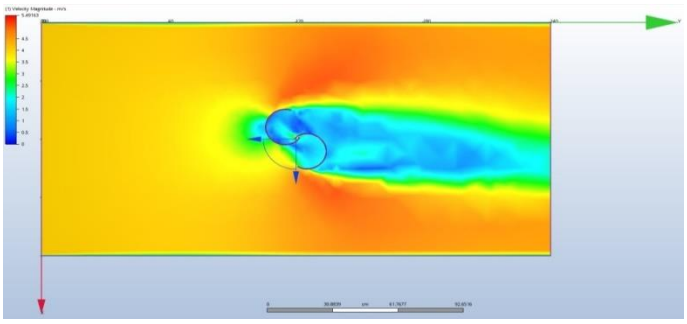

Fig -6: Velocity distribution of Model 9 wind speed of 3m/s

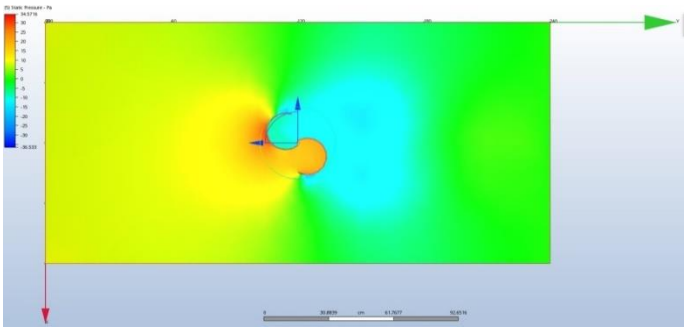

Fig -7: Pressure distribution of Model 9 at wind speed of 6m/s

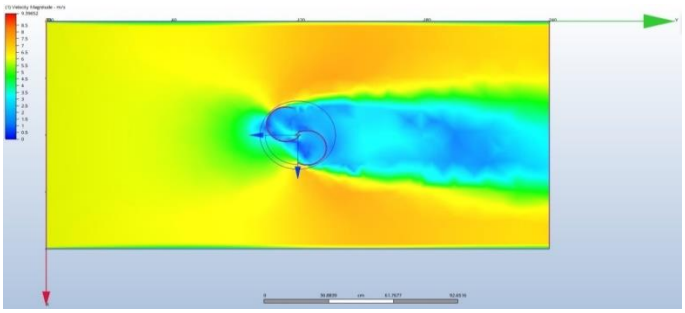

Fig -8: Velocity distribution of Model 9 wind speed of 6m/s

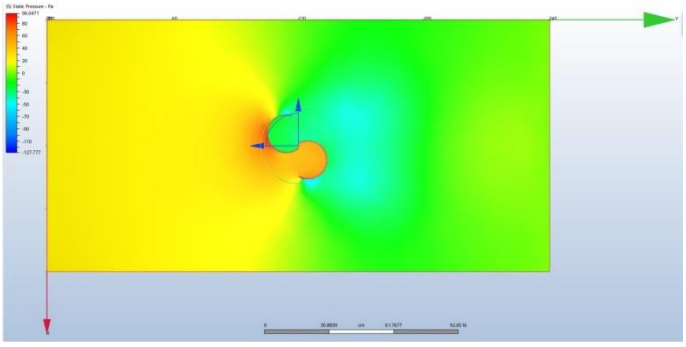

Fig -9: Pressure distribution of Model 9 at wind speed of 10m/s

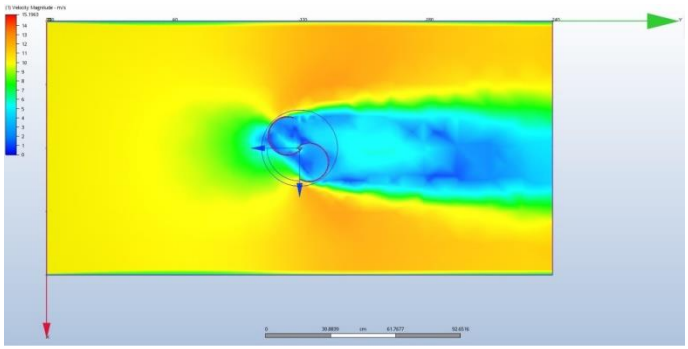

Fig -10: Velocity distribution of Model 9 wind speed of 10m/s

3. CONCLUSIONS

In this study, numerical investigations were carried out to study the effect of bucket angle on the static torque of the rotors. This study compares different designs of rotor characterized by the bucket arc angles equal to 80°, 90°, 100°, 125°, and 150° when keeping constants the others geometrical parameters. In these conditions, the second case considers as a classical Savonius wind turbine rotor. The following conclusions can be given from the obtained results:

- It is found that the end plate and bucket angle are able to increase the static torque of the rotors.
- It is observed that the rotor with bucket angle of 150° has high torque compared to other rotors.
- The use of both upper and lower circular end plates significantly increased the static torque by 42% compared with no end plate.

ACKNOWLEDGEMENT

The authors would like to thank the Faculty of Engineering especially the Mechanical Engineering Department at Near East University for their support and encouragement.

REFERENCES

[1] Mathew, S. (2006). Wind energy: Fundamentals, resource analysis, and economics. Berlin: Springer.

[2] Hemami , A. (2012). Wind Turbine Technology, Unite State of America. Cengage Learning.

[3] Savonius SJ. The S-rotor and its application. Mech Eng 1931; 53:333-8.

[4] Twidwell JW, Weir AD. Renewable energy resources. The University Press Cambridge, Britain; 1985. 1-411.

[5] Eldridge FR. Wind machines. Newyork: Van Nostrand; 1980. 1-214.

[6] Kacprzak, K., Liskiewicz, G., & Sobczak, K. (2013). Numerical investigation of conventional and modified Savonius wind turbines. *Renewable Energy*, *60*, 578-585. doi:10.1016/j.renene.2013.06.009

[7] Roy, S., & Saha, U. K. (2015). Wind tunnel experiments of a newly developed two-bladed Savonius-style wind turbine. *Applied Energy*, *137*, 117-125. doi:10.1016/j.apenergy.2014.10.022

[8] Sharma, S., & Sharma, R. K. (2016). Performance improvement of Savonius rotor using multiple quarter blades – A CFD investigation. *Energy Conversion and Management*,*127*, 43-54. doi:10.1016/j.enconman.2016.08.087

[9] Mohamed, M., Janiga, G., Pap, E., & Thévenin, D. (2011). Optimal blade shape of a modified Savonius turbine using an obstacle shielding the returning blade. *Energy Conversion and Management*, *52*(1), 236-242. doi:10.1016/j.enconman.2010.06.070

[10] Mahmoud, N., El-Haroun, A., Wahba, E., & Nasef, M. (2012). An experimental study on improvement of Savonius rotor performance. *Alexandria Engineering Journal*, *51*(1), 19-25. doi:10.1016/j.aej.2012.07.003

[11] Tartuferi, M., D'Alessandro, V., Montelpare, S., & Ricci, R. (2015). Enhancement of Savonius wind rotor aerodynamic performance: a computational study of new blade shapes and curtain systems. *Energy*, *79*, 371-384. doi:10.1016/j.energy.2014.11.023

[12] Lee, J., Lee, Y., & Lim, H. (2016). Effect of twist angle on the performance of Savonius wind turbine. *Renewable Energy*, *89*, 231-244. doi:10.1016/j.renene.2015.12.012

[13] Nasef, M., El-Askary, W., AbdEL-hamid, A., & Gad, H. (2013). Evaluation of Savonius rotor performance: Static and dynamic studies. *Journal of Wind Engineering and Industrial Aerodynamics*, *123*, 1-11. doi:10.1016/j.jweia.2013.09.009

[14] Saha, U., Thotla, S., & Maity, D. (2008). Optimum design configuration of Savonius rotor through wind tunnel experiments. *Journal of Wind Engineering and Industrial Aerodynamics*, *96*(8-9), 1359-1375. doi:10.1016/j.jweia.2008.03.005

[15] Roy, S., & Saha, U. K. (2015). Wind tunnel experiments of a newly developed two-bladed Savonius-style wind turbine. *Applied Energy*, *137*, 117-125. doi:10.1016/j.apenergy.2014.10.022

[16] Kang, C., Liu, H., & Yang, X. (2014). Review of fluid dynamics aspects of Savonius-rotor-based vertical-axis wind rotors. *Renewable and Sustainable Energy Reviews*, *33*, 499-508. doi:10.1016/j.rser.2014.02.011

[17] Akwa, J. V., Alves da Silva Júnior, G., & Petry, A. P. (2012). Discussion on the verification of the overlap ratio influence on performance coefficients of a Savonius wind rotor using computational fluid dynamics. *Renewable Energy*, *38*(1), 141-149. doi:10.1016/j.renene.2011.07.013

[18] Driss, Z., Damak, A., & Abid, M. S. (2015). Evaluation of the Savonius Wind Rotor Performance for Different External Overlap Ratios. *International Journal of Fluid Mechanics & Thermal Sciences*, *1*(1), 14. doi:10.11648/j.ijfmts.20150101.13

[19] Mohamed, M., Janiga, G., Pap, E., & Thévenin, D. (2010). Optimization of Savonius turbines using an obstacle shielding the returning blade. *Renewable Energy*, *35*(11), 2618-2626. doi:10.1016/j.renene.2010.04.007

[20] Wenehenubun, F., Saputra, A., & Sutanto, H. (2015). An Experimental Study on the Performance of Savonius Wind Turbines Related With The Number Of Blades. Energy Procedia, 68, 297-304. doi:10.1016/j.egypro.2015.03.259

[21] Roy, S., & Saha, U. K. (2013). Review on the numerical investigations into the design and development of Savonius wind rotors. *Renewable and Sustainable Energy Reviews*, *24*, 73-83. doi:10.1016/j.rser.2013.03.060

[22] Kianifar, A., Anbarsooz, M., & Javadi, M. (2010). Blade Curve Influences on Performance of Savonius Rotors: Experimental and Numerical. *ASME 2010 3rd Joint US-European Fluids Engineering Summer Meeting: Volume 1, Symposia – Parts A, B, and C*. doi:10.1115/fedsm-icnmm2010-30919

[23] Kianifar, A., & Anbarsooz, M. (2011). Blade curve influences on the performance of Savonius rotors: experimental and numerical. *Proceedings of the Institution of Mechanical Engineers, Part A: Journal of Power and Energy*, *225*(3), 343-350. doi:10.1177/2041296710394413

[24] Lin, C., & Klimina, L. A. (2014). CFD simulation and analysis for Savonius rotors with different blade configuration. doi:10.1063/1.4904626

[25] Muscolo, G. G., & Molfino, R. (2014). From Savonius to Bronzinus: A Comparison among Vertical Wind Turbines. *Energy Procedia*, *50*, 10-18. doi:10.1016/j.egypro.2014.06.002

[26] Driss, Z., Mlayeh, O., Driss, S., Driss, D., Maaloul, M., & Abid, M. S. (2015). Study of the bucket design effect on the turbulent flow around unconventional Savonius wind rotors.*Energy*, *89*, 708-729. doi:10.1016/j.energy.2015.06.023

[27] Frikha, S., Driss, Z., Ayadi, E., Masmoudi, Z., & Abid, M. S. (2016). Numerical and experimental characterization of multi-stage Savonius rotors. *Energy*, *114*, 382-404. doi:10.1016/j.energy.2016.08.017

[28] Driss, Z., Mlayeh, O., Driss, S., Maaloul, M., & Abid, M. S. (2016). Study of the incidence angle effect on the aerodynamic structure characteristics of an in curved Savonius wind rotor placed in a wind tunnel. *Energy*, *113*, 894-908. doi:10.1016/j.energy.2016.07.112

[29] Saha, U., Thotla, S., & Maity, D. (2008). Optimum design configuration of Savonius rotor through wind tunnel experiments. Journal of Wind Engineering and Industrial Aerodynamics, 96(8-9), 1359-1375. doi:10.1016/j.jweia.2008.03.005

BIOGRAPHIES

Sarkar Arzasher Mohammed Balak graduated from Near East University in Mechanical Engineering department located in Cyprus. He has experience on CFD and FEM by using several different softwares. He has interest in engineering design.

Khedr Halimeh is a graduate student from Near East university in the department of mechanical engineering. His main interest is designing and implementing modern engineering technology.

Mohammad ALHafez is a graduate student from Near East university in the department of mechanical engineering.

Assist. Prof. Dr. Hüseyin ÇAMUR received his Ph.D degree in 2000, in Mechanical Engineering Department, Engineering Faculty, Fırat University. He has been awarded the assistant professorship in 2001.

Dr. Youssef Kassem received his Ph.D. degree in Mechanical Engineering from Near east University (2017 January, TRNC, Turkey). Currently, He is a lecturer for various engineering subjects in the faculty. His current researches focuses are on are analyzing the renewable sources such as wind, solar and biofuel in Cyprus.